separations

MDPI

Article

Mechanical Activation of Silicate Rocks for CO_2 Adsorption: Decoupling Structural Modification and Adsorption–Desorption Performance

Yizhuo Li [1,2], Duoxueer Jia [1], Jiajie Li [1,2,*], Yafeng Fu [2], Pengyun Xu [3] and Fengming Xi [2]

[1] School of Resources and Safety Engineering, University of Science and Technology Beijing, Beijing 100083, China; liyizhuo@ustb.edu.cn (Y.L.)
[2] Institute of Mineral Resources, University of Science and Technology Beijing, Beijing 100083, China
[3] China National Engineering Research Center for Electronic Waste Recycling, Jingmen 448000, China
* Correspondence: jiajieli@ustb.edu.cn

Abstract

Mechanical activation modifies silicate rocks and provides opportunities for evaluating mineral-derived CO_2 sorbents. This study examines the relationship among particle refinement, diffraction changes, and pressure-dependent CO_2 loading and release in granite, basalt, and peridotite subjected to dry planetary milling for 0–120 min. Particle-size analysis, X-ray diffraction, and pure-CO_2 measurements at 298.15 K revealed material-dependent responses. Peridotite continued to become finer with milling, whereas its 1-bar loading peaked after 30 min and subsequently declined. Relative to the prepared baseline, 30 min milling increased peridotite uptake by 68.5% at 0.15 bar and 8.7% at 1 bar, while decreasing release over the measured 1.0–0.1 bar descending branch by 8.6%. These observations support evaluating milling conditions against pressure-specific loading and release objectives. The results characterize samples conditioned at 26 °C for 120 min; pretreatment sensitivity, residual moisture, and branch equilibration require further validation. The study provides preliminary comparisons for selecting treatments for subsequent sorption validation and mineralization experiments.

Keywords: CO_2 adsorption–desorption; mechanical activation; silicate rocks; surface modification; sustainable resource utilization

1. Introduction

Silicate minerals have attracted interest as feedstocks for integrating CO_2 capture with mineral carbonation because their surfaces can adsorb CO_2 and their constituent cations can participate in carbonate formation [1–3]. Mechanical activation offers a means of modifying these properties through particle fracture, surface generation, and changes in crystal structure. Its effectiveness, however, depends on how these changes influence the relevant gas–solid interactions. Increasing the extent of grinding does not necessarily produce a proportional improvement in adsorption, and a higher adsorption capacity does not necessarily provide greater CO_2 release during regeneration.

Previous studies by Li and Hitch [1,2] showed that mineral treatment affects surface-area-normalized CO_2 uptake and regeneration behavior in addition to total adsorption capacity. These observations indicate that the adsorption response is governed by more than the amount of exposed surface. Water and CO_2 interactions vary with the mineral interface [4], while calculations for forsterite show that surface termination influences

Check for updates

Academic Editor: Guojie Zhang

Received: 27 October 2026
Revised: 23 November 2026
Accepted: 23 November 2026
Published: 26 November 2026

Copyright: © 2026 by the authors. Licensee MDPI, Basel, Switzerland. This article is an open access article distributed under the terms and conditions of the Creative Commons Attribution (CC BY) license.

CO_2 binding [5]. Furthermore, nitrogen BET surface area represents accessibility under nitrogen measurement conditions and cannot be equated directly with the abundance of sites accessible to CO_2 at a different temperature [6]. The relationship between surface development and CO_2 adsorption must therefore be evaluated experimentally.

Mechanical activation also changes the structural state of the mineral independently of its external dimensions. Enhanced olivine dissolution has been observed despite aggregation and limited increases in BET area [7], and XRD analysis reveals microstructural changes that are not captured by particle-size measurements [8]. Kleiv and Thornhill [9] similarly showed that the increase in olivine reactivity can exceed that attributable to surface-area development. Although these studies establish the importance of structural activation, the correspondence among particle refinement, diffraction changes, surface development, and pressure-dependent CO_2 adsorption remains insufficiently resolved. In particular, assessment based on maximum surface area or a single adsorption pressure can obscure differences between enhanced loading and improved regeneration. The remaining gap concerns the joint evaluation of these responses within a common milling series: structural or dissolution-based measures of activation do not establish pressure-specific gas loading or the amount released during depressurization. The present comparison therefore focuses on particle-size and diffraction descriptors alongside mass-specific CO_2 loading and release.

Granite, basalt, and peridotite were milled under identical operating conditions for four treatment durations. Particle-size analysis, multi-peak XRD characterization, and pure-CO_2 measurements were combined to compare structural descriptors with loading at 0.15 and 1.00 bar and release over a common descending-branch interval. The contribution is a descriptive assessment of how treatment rankings depend on the measured property and pressure window.

These comparisons distinguish treatments associated with greater measured loading from those associated with greater release within the experimental pressure interval. Their relevance to reactive grinding and mineral carbonation motivates subsequent measurements of reaction performance and carbon retention [10–14].

2. Materials and Methods

2.1. Materials and Mechanical Treatment

Granite (G), basalt (B), and peridotite (O) were investigated at four milling durations. Sample labels G-0 min to G-120 min, B-0 min to B-120 min, and O-0 min to O-120 min identify the rock series and treatment time. The corresponding analytical identifiers were A1–A4, B1–B4, and C1–C4, respectively. Particle-size, XRD, and gas-adsorption measurements were matched by these sample identifiers. The starting materials were rock blocks used for laboratory experiments. Before the treatment series, each rock material was preliminarily ground for 20 min to a nominal fineness of approximately 400 mesh to simulate the particle fineness of tailings, followed by oven drying. The 0 min designation refers to the baseline material obtained after this common preparation step. The subsequent 30, 60, and 120 min treatments represent additional milling durations.

Dry milling was conducted in air using a high-energy, four-station vertical planetary ball mill (XQM-2 type, nominal capacity of 2 L; Changsha Tianchuang Powder Technology Co., Ltd., Changsha, China) equipped with four 500 mL stainless-steel jars at a milling-jar self-rotation speed of 500 rpm and a ball-to-powder mass ratio of 7:1. Before treatment, the starting material from each rock series was divided into four separate aliquots corresponding to milling durations of 0, 30, 60, and 120 min, with each milled aliquot processed independently in its own jar. For each treatment, 64.3 g of sample was combined with 450 g of zirconia balls. Zirconia balls with diameters of 5, 8, 10, 12, and 15 mm were mixed at a mass ratio of 6:5:5:2:2, respectively. The jars were sealed under ambient air without vacuum

treatment or inert-gas purging. To limit heat accumulation, each 5 min milling period was followed by 5 min of ambient cooling, although the jar temperature was not monitored directly. Milling durations were 0, 30, 60, and 120 min, with the reported durations representing cumulative active milling time and excluding the intervening cooling periods; the unmilled material served as the reference for each rock series. Initial particle-size distributions differed among the three materials; treatment responses were therefore evaluated primarily relative to the corresponding unmilled sample. The reported comparisons comprise three rock types and four treatment durations per rock type. Milling was performed before, rather than during, CO_2 exposure; the adsorption results therefore characterize the post-milling materials and not carbon uptake during reactive grinding.

2.2. Particle Size and Diffraction Characterization

Particle-size distributions were determined by wet laser diffraction in water using a Bettersize 2600 instrument (Bettersize Instruments Ltd., Dandong, China). The volume median diameter, D_{50}, is used to compare particle refinement. Geometrical surface areas calculated from the particle-size analysis are not substituted for gas-adsorption surface areas.

XRD patterns were acquired using an Ultima IV diffractometer (Rigaku Corporation, Tokyo, Japan) with Cu radiation at 40 kV and 40 mA. Measurements covered 3–80° 2θ with a step size of 0.02° and a counting time of 0.6 s per step. Peak positions and widths were obtained using JADE (version 9.0) with a 51-point parabolic filter, a threshold of 5.0, a cutoff of 0.1%, and peak-top summit evaluation. A wavelength of 1.54056 Å was used to calculate d-spacings. Relative intensities were normalized separately for each pattern.

Recurring diffraction features were matched by position within each rock series, and their full widths at half maximum (FWHM) were compared across milling durations (Table 1). Features were designated by approximate 2θ position because overlapping reflections in these multiphase materials preclude unique phase assignments from the peak-search results alone. FWHM values were obtained from the original laboratory peak tables without correction for instrumental broadening. These uncorrected widths are empirical descriptors of diffraction features; quantification of coherent-domain size, lattice strain, amorphous fraction, and structural disorder requires instrument-corrected whole-pattern analysis.

Table 1. Matched diffraction-feature widths across the milling schedule.

Series	Feature (° 2θ)	0 min	30 min	60 min	120 min
Granite	20.84	0.173	0.190	0.173	0.171
Granite	26.62	0.167	0.162	0.150	0.151
Granite	27.48	0.123	0.190	0.154	0.177
Basalt	10.46	0.149	0.143	0.150	0.153
Basalt	28.50	0.133	0.151	0.154	0.157
Basalt	32.92	0.145	0.199	0.206	0.222
Basalt	34.38	0.174	0.230	0.237	0.262
Basalt	35.00	0.176	0.193	0.238	0.250
Peridotite	32.29	0.086	0.152	0.161	0.154
Peridotite	35.64	0.124	0.224	0.244	0.223
Peridotite	36.44	0.109	0.193	0.168	0.170
Peridotite	52.46	0.086	0.302	0.328	0.278
Peridotite	66.96	0.091	0.224	0.342	0.258

2.3. Gas Adsorption and Pretreatment Scope

CO_2 adsorption–desorption was measured at 298.15 K using a 3H-2000PS2 static volumetric analyzer (Beishide Instrument Technology (Beijing) Co., Ltd., Beijing, China)

and CO_2 of at least 99.9% purity. Samples were conditioned at 26 °C for 120 min using a common protocol across all milling treatments. These conditions may have favored the retention of moisture and previously adsorbed species on the mineral surfaces, potentially influencing adsorption-site accessibility and the measured CO_2 response. The reported loadings therefore characterize the materials in this conditioned state. Sample-specific thermogravimetric analysis, complementary characterization, and adsorption measurements following controlled pretreatment at different temperatures are required to establish a suitable conditioning range and quantify pretreatment sensitivity.

Exploratory nitrogen measurements at 77.3 K used the same recorded pretreatment of 26 °C for 120 min. Reliable textural characterization requires adequate removal of pre-adsorbed species under documented conditions [6]. Since the extent of outgassing remains unvalidated, nitrogen-derived BET areas, pore volumes, and pore-size interpretations are excluded from the present results. The analysis is restricted to particle-size and diffraction descriptors and mass-specific CO_2 measurements, pore classification and surface-area-normalized interpretation require validated textural measurements.

2.4. Pressure Interpolation and Release Calculation

CO_2 pressure was calculated as $P = rP_{ref}$, where r is the tabulated pressure ratio and P_{ref} is approximately 1.015 bar. Volumetric uptake was converted to mass-specific uptake using:

$$q_m = q_V \frac{M_{CO_2}}{V_m} \quad (1)$$

Here, q_m and q_V denote uptake in mg g^{-1} and mL g^{-1}, respectively; $M_{CO_2} = 44.01$ mg $mmol^{-1}$ and $V_m = 22.414$ mL $mmol^{-1}$. Gas volumes were referenced to 0 °C and 1 atm, giving a volumetric-to-mass conversion factor of 1.9635 mg mL^{-1}. Equilibrium was defined as pressure variation within 1% over 60 s, with both instrument extension coefficients set to 5. Pressure was measured over 0–1000 Torr with a specified accuracy of ±0.15%, and free-space volume was determined using helium. A propagated uncertainty assessment requires clarification of the accuracy basis, together with calibration records and independent repeatability measurements.

For a target pressure P^* bracketed by two points on the same branch, uptake was calculated as:

$$q(P^*) = q_1 + (q_2 - q_1)\frac{P^* - P_1}{P_2 - P_1} \quad (2)$$

Adsorption loadings at 1.00 and 0.15 bar were interpolated independently within the measured adsorption branch. These values provide comparisons at two pure-CO_2 pressures.

Desorption release over a common pressure interval was calculated solely from the descending branch:

$$\Delta q_{des} = q_{des}(1.00\ \text{bar}) - q_{des}(0.10\ \text{bar}) \quad (3)$$

Both endpoints used to calculate release lie within the measured descending branch. The adsorption run reached approximately 1.005–1.011 bar; the descending measurements terminate near 0.1 bar, above the initial adsorption pressure. The low-pressure closure point was therefore outside the measured descending range. This finite endpoint explains why closure was not tested, rather than establishing the physical cause of branch separation. The pressure-stability criterion is an operational stopping rule; thermodynamic equilibration requires additional dwell-time tests. Residual moisture, slow transport, surface interactions, and instrumental effects remain possible contributors. Release is reported as a difference along this single measured branch and requires repeated-cycle validation for regeneration assessment.

3. Results

3.1. Particle Refinement and Multi-Peak Diffraction Changes

Particle refinement occurred predominantly within the first 30 min for granite and basalt (Figure 1a). Granite D_{50} decreased from 23.63 to 3.220 µm, then increased to 3.676 µm at 120 min. Basalt decreased from 26.04 to 3.491 µm, followed by values near 4.54 µm at 60 and 120 min. These later increases are consistent with a change in the balance between fragmentation and aggregation.

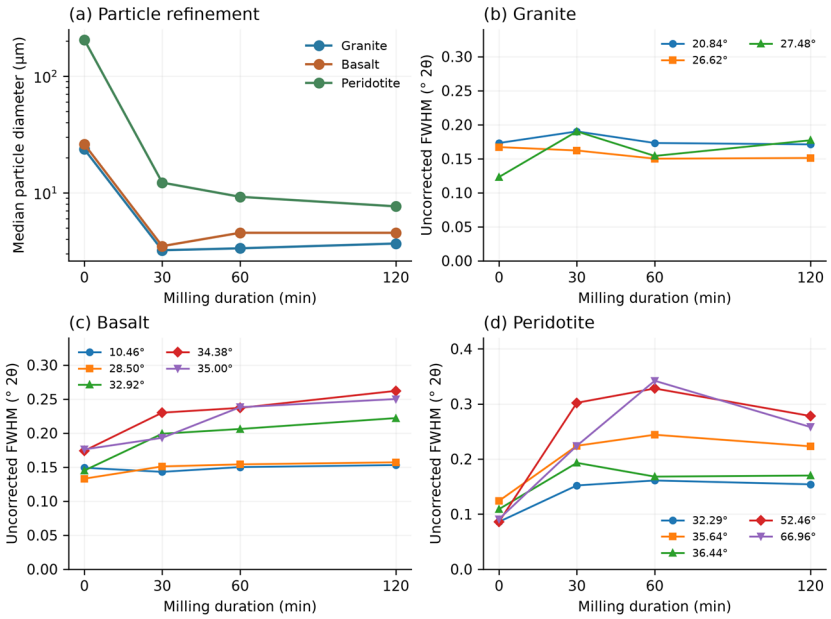


Figure 1. Effect of milling duration on (**a**) volume median particle diameter and (**b**–**d**) FWHM of matched diffraction features in granite, basalt, and peridotite.

Peridotite underwent continued particle refinement throughout the milling period. Its D_{50} decreased from 204.7 µm before milling to 12.23, 9.245, and 7.655 µm after 30, 60, and 120 min, respectively. This monotonic reduction contrasted with the nonmonotonic response of measured CO_2 loading.

Diffraction features responded differently to milling (Figure 1 and Table 1). In granite, FWHM near 26.6° decreased from 0.167° to 0.151° between 0 and 120 min, whereas FWHM near 27.48° increased from 0.123° to 0.177°. The feature near 20.84° changed only modestly, indicating that the structural response was reflection-dependent.

In basalt, FWHM near 10.46° remained approximately constant, changing from 0.149° to 0.153°. In contrast, the features near 32.92°, 34.38°, and 35.00° broadened from 0.145°, 0.174°, and 0.176° to 0.222°, 0.262°, and 0.250°, respectively. These increases correspond to approximately 53%, 51%, and 42% broadening after 120 min.

All five selected peridotite features were broader after milling than in the unmilled material, but their maximum widths occurred at different durations. The feature near 36.44° was broadest after 30 min, whereas those near 35.64°, 52.46°, and 66.96° were broadest after 60 min. FWHM near 52.46° increased from 0.086° to 0.302° and 0.328° at 30 and 60 min, then decreased to 0.278° at 120 min. The corresponding values near 66.96° were 0.091°, 0.224°, 0.342°, and 0.258°. Changes in the measured diffraction features persisted beyond the treatment associated with maximum adsorption.

3.2. CO_2 Adsorption Loading and Pressure Dependence

Peridotite had the highest 1-bar adsorption loading at every matched milling duration (Figure 2 and Table 2). Its loading increased from 2.710 mg g^{-1} before milling to 2.944 mg g^{-1} after 30 min, an 8.7% increase, then fell to 1.910 and 1.166 mg g^{-1} after 60 and 120 min. The final value was 57.0% below the unmilled loading. This decline occurred despite continued reduction in median particle diameter.

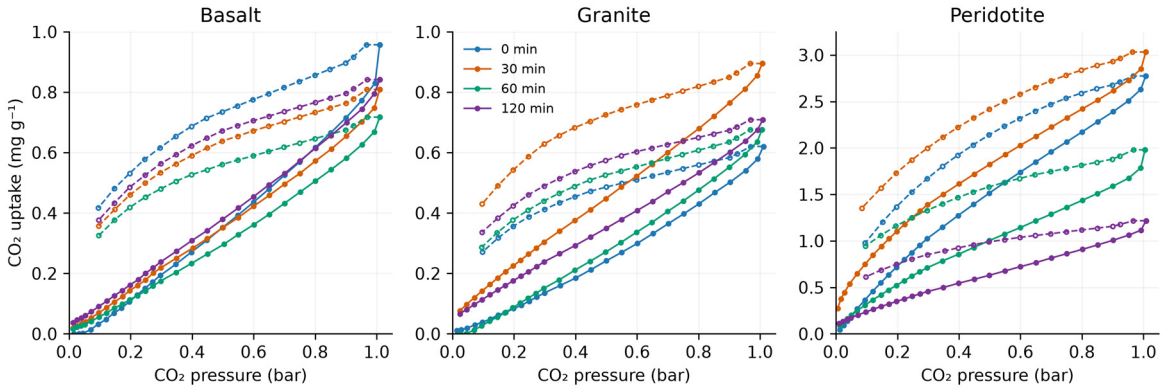


Figure 2. CO_2 adsorption–desorption isotherms at 298.15 K. Filled symbols and solid lines denote adsorption; open symbols and dashed lines denote desorption. Colors identify milling durations. Basalt and granite use a 0–1 mg g^{-1} vertical scale. Descending branches terminate near 0.1 bar; closure at the initial adsorption pressure was outside the acquisition range. Curves connect the recorded points and represent single measurements under the stated conditioning and equilibration protocol.

Table 2. CO_2 loading and desorption descriptors at 298.15 K.

Sample	q_{ads} (0.15 Bar)	q_{ads} (1.00 Bar)	q_{des} (1.00 Bar)	q_{des} (0.10 Bar)	Δq_{des} (1–0.1 Bar)
B-0 min	0.071	0.873	0.957	0.423	0.534
B-30 min	0.107	0.774	0.809	0.361	0.448
B-60 min	0.086	0.689	0.717	0.329	0.389
B-120 min	0.128	0.815	0.842	0.381	0.461
G-0 min	0.063	0.596	0.620	0.273	0.347
G-30 min	0.187	0.878	0.895	0.434	0.461
G-60 min	0.058	0.660	0.676	0.292	0.385
G-120 min	0.147	0.692	0.709	0.340	0.369
O-0 min	0.563	2.710	2.775	0.998	1.777
O-30 min	0.948	2.944	3.032	1.407	1.625
O-60 min	0.427	1.910	1.980	0.954	1.026
O-120 min	0.298	1.166	1.217	0.617	0.600

All loadings and descending-branch release values are expressed in mg g^{-1}. Loadings are linearly interpolated within the indicated branch. Descending-branch release is the difference between descending loadings at 1.00 and 0.10 bar.

Granite loading increased from 0.596 to 0.878 mg g^{-1} after 30 min, a 47.2% increase, and subsequently decreased to 0.660–0.692 mg g^{-1}. Basalt showed lower 1-bar loading after each milling treatment: 0.774, 0.689, and 0.815 mg g^{-1} at 30, 60, and 120 min, respectively, compared with 0.873 mg g^{-1} before milling.

The effect of milling varied with pressure. At 0.15 bar, O-30 min adsorbed 0.948 mg g^{-1}, compared with 0.563 mg g^{-1} for O-0 min, an increase of approximately 68.5%. The increase at 1 bar was only 8.7%. Milled basalt also exhibited greater loading at 0.15 bar than the unmilled material despite its lower loading at 1 bar. These differences indicate that milling altered the shape of the pure-CO_2 adsorption response.

3.3. Metric-Dependent Selection of Milling Conditions

All CO_2 records showed separation between their adsorption and desorption branches. At 0.10 bar on the desorption branch, peridotite retained 0.998, 1.407, 0.954, and 0.617 mg g^{-1} for the four increasing milling durations. Release between 1.00 and 0.10 bar was greatest for O-0 min, at 1.777 mg g^{-1}, and decreased to 1.625, 1.026, and 0.600 mg g^{-1}. Thus, the 30 min sample increased adsorption loading but reduced release over this interval by 8.6% relative to the unmilled material.

Basalt release ranged from 0.389 to 0.534 mg g^{-1}, with the unmilled material again giving the highest value. Granite release ranged from 0.347 to 0.461 mg g^{-1}, with the highest value after 30 min. Adsorption loading and desorption release therefore selected the same tested duration for granite and basalt, but different durations for peridotite.

Granite exhibited the largest measured 1-bar loading and release after 30 min. Basalt exhibited the largest values for both descriptors in the prepared baseline. Peridotite exhibited its largest loading after 30 min and its largest release in the baseline. These rankings are descriptive comparisons within the measured protocol.

4. Discussion

4.1. Decoupling of Structural Modification and CO_2 Adsorption

Particle refinement, diffraction changes, and CO_2 loading followed different trajectories. In peridotite, continued refinement beyond 30 min accompanied declining loading. Particle size thus provides a structural descriptor whose relationship to sorption must be evaluated under specified measurement conditions.

The diffraction response further separates structural modification from adsorption performance. Between 30 and 60 min, peridotite loading decreased by 35.1%, although the features near 52.46° and 66.96° broadened. Other features, including that near 36.44°, narrowed during the same interval. Basalt also exhibited broadening at several higher-angle features after 120 min while retaining less CO_2 at 1 bar than the unmilled material. These differences show that increased width of a selected reflection cannot be used as a direct predictor of adsorption enhancement.

Particle-size analysis and XRD probe different material properties: dispersed particle dimensions and diffraction features influenced by coherent domains, strain, and overlapping reflections. CO_2 loading additionally reflects the conditioned surface and measurement history. Li and Hitch [8] demonstrated the value of whole-pattern analysis for microstructural interpretation, while Haug et al. [15] related mechanical activation to dissolution behavior. In the present study, the structural descriptors support comparison of milling responses; their connection to adsorption mechanisms requires complementary surface and kinetic measurements.

4.2. Pressure-Dependent Adsorption and Desorption Behavior

Peridotite displayed a pressure-dependent loading response. After 30 min of milling, uptake increased from 0.563 to 0.948 mg g^{-1} at 0.15 bar and from 2.710 to 2.944 mg g^{-1} at 1 bar. The ratio of these two loadings increased from 0.208 to 0.322. This describes a change in the measured pressure response. Establishing its origin requires pretreatment validation, equilibration tests, and measurements that distinguish surface interactions from transport effects.

The desorption response further separates enhanced loading from improved release. For peridotite, 30 min milling increased 1-bar adsorption but reduced CO_2 release over the descending 1.0–0.1 bar interval from 1.777 to 1.625 mg g^{-1}, a decrease of 8.6%. The fraction of descending-branch loading retained at 0.1 bar increased from 0.360 to 0.464. Greater retention during depressurization therefore outweighed the increase in initial

loading within this pressure window. This observation is consistent with the importance of regenerability emphasized by Li and Hitch [1], while the molecular origin of the retention remains unresolved.

Treatment selection depends on the intended measurement objective. Among the peridotite samples, 30 min milling gave the largest measured 1-bar loading, whereas the baseline gave the largest release over 1.0–0.1 bar. These conditional rankings motivate replicated measurements at defined conditioning and equilibration settings before process optimization.

The measured branch separation does not uniquely identify chemisorption. Binding heterogeneity, restricted transport, residual water, and equilibration behavior can also produce retention during depressurization. Moreover, Δq_{des} characterizes a single desorption path rather than repeated-cycle working capacity. The present results establish the divergence between loading and release under pure-CO_2 conditions; their extension to cyclic separation requires mixed-gas and repeated-cycle measurements. The measurement at 0.15 bar characterizes pure-CO_2 adsorption. Assessment of competitive adsorption and mixed-gas selectivity requires mixture measurements, while regeneration stability and cyclic working capacity require repeated adsorption–desorption cycles.

4.3. Implications for Grinding-Assisted Carbon Mineralization

The separation between structural modification and gas adsorption has implications for grinding-assisted carbon mineralization. A decrease in post-milling adsorption does not necessarily imply diminished mineral reactivity. Sandvik et al. [7] reported enhanced dissolution of mechanically activated olivine despite aggregation, while Li and Hitch [3] demonstrated improved aqueous carbonation following mechanical activation. These findings indicate that the structural changes responsible for dissolution or carbonate formation need not maximize dry-gas adsorption. Together with the dissolution studies [7,9,15], this comparison indicates that an activation criterion established for a reactive aqueous process cannot be transferred directly to dry-gas adsorption. The present results extend that distinction by showing that even adsorption loading and release can favor different treatments within a single material series.

The timing of CO_2 exposure may be particularly important. Milling in air, as used here, separates surface generation from the subsequent CO_2 adsorption measurement. Reactive grinding instead exposes newly generated interfaces to CO_2 during mechanical treatment. Incorporation of atmospheric CO_2 during silicate grinding was reported by Kalinkina et al. [10], and carbonate formation has been observed during wet and CO_2-flow milling of olivine [11,13]. Fresh surfaces may undergo reaction, hydration, or reconstruction before a post-milling adsorption test, so that test need not capture the full carbon uptake during reactive grinding. Sanna et al. [16] also demonstrated gas-phase chemical effects during granite fracture and friction, including ozone generation in oxygen, further illustrating the influence of the milling atmosphere on mechanochemical reactions.

Stillings et al. [14] showed that granite and basalt milled under CO_2 at 4 bar for 2.5 h incorporated more carbon than predicted from the weighted responses of their constituent minerals. The rocks retained 98% and 96% of the incorporated carbon, respectively, after 24 h of water leaching. Carbon analysis and thermal desorption, together with the absence of identified new carbonate minerals, supported an interface-associated chemical trapping mechanism. Their proposed roles for stress concentration, charged species, and deformation-assisted diffusion provide a basis for investigating polymineralic interfaces during reactive grinding. These mechanisms remain distinct from the pressure-dependent adsorption behavior measured here and cannot be inferred from XRD broadening alone.

For conventional carbonate formation, the overall reaction of the Mg endmember can be represented as:

$$Mg_2SiO_4 + 2CO_2 \rightarrow 2MgCO_3 + SiO_2 \quad (4)$$

This stoichiometric balance may proceed through hydration, dissolution, and precipitation, with hydrated carbonate intermediates or products depending on reaction conditions [4,13]. Attrition can renew reactive surfaces during aqueous carbonation, as demonstrated by Julcour et al. [12], while ex situ carbonation studies establish the importance of controlled reaction conditions [17]. Thus, continued grinding may benefit mineral reaction even after dry-gas adsorption has declined. Demonstrating this behavior in the present materials would require direct measurements of dissolution and carbonate formation.

Peridotite milled for 30 and 60 min provides a useful comparison for investigating this relationship: the former exhibits greater adsorption, whereas the latter shows broader selected diffraction features. Comparing these treatments during aqueous carbonation and CO_2-assisted milling would establish whether the divergence between structure and adsorption also extends to reaction performance. Immediate CO_2 exposure after inert-gas milling could further distinguish the effects of surface generation from those of exposure during grinding. Carbon balances, product characterization, and retention measurements would be required to separate reversible adsorption, carbonate formation, and other persistent trapping mechanisms.

The engineering value of grinding-assisted capture ultimately depends on persistent carbon retention relative to energy use and associated emissions. Where grinding is already part of mineral processing, assessment should include the additional energy required for CO_2 supply, residence time, water handling, and downstream treatment. Dedicated carbon-management milling requires the full comminution energy to be included. Neither reversible adsorption nor calculated carbonate capacity represents a measured permanent-storage yield. The present results therefore provide criteria for selecting and comparing mechanically activated feedstocks, while reaction and energy balances are needed to establish their mineralization benefit.

4.4. Limitations and Future Research

The principal limitation is the absence of independent milling and adsorption replicates. The observed trends describe the measured treatments, but uncertainty in rankings and small differences cannot be quantified. Initial particle-size distributions also differed among rock types, and equal milling durations did not necessarily correspond to equal specific energy inputs. Replicated preparations, energy measurements, and standardized pretreatment would strengthen comparisons among materials. At least three independent milling preparations per treatment, with corresponding adsorption measurements, are needed to assess between-preparation variability. As only one preparation was tested per treatment, the reported 8.7% increase in loading and 8.6% decrease in release for peridotite after 30 min should be interpreted as descriptive trends requiring independent validation.

Structural interpretation remains limited by uncorrected peak widths and the lack of quantitative phase analysis. Instrument-corrected whole-pattern analysis is needed to distinguish crystallite-size, strain, peak-overlap, and amorphous contributions, while quantitative mineralogy and elemental analysis would clarify phase-specific responses and reactive-cation availability. Detailed collection and drying records would further improve reproducibility.

Validated outgassing and repeated nitrogen measurements are required before assessing surface area, pore volume, pore-size distributions, or mesoporosity. For CO_2, temperature-dependent pretreatment tests, extended low-pressure desorption, longer equilibration periods, and repeated cycles would distinguish conditioning effects and measure-

ment history from persistent retention. Humidity-controlled measurements and surface spectroscopy could further test the role of water and surface chemistry. These measurements are prerequisites for mechanistic interpretation of the observed branch separation.

Repeated mixed-gas cycles are needed to establish separation performance, while dissolution tests and carbon-balanced product analysis are required to evaluate mineralization. The distinction is important because a milling condition that improves one response may reduce another. The present comparisons establish this dependence within the investigated treatment and pressure ranges.

5. Conclusions

Under the specified conditioning and measurement protocol, granite, basalt, and peridotite exhibited distinct relationships among particle refinement, diffraction changes, and mass-specific CO_2 loading. Peridotite continued to refine beyond 30 min while its measured loading declined. The structural and sorption descriptors therefore support complementary assessments of treatment response.

Peridotite treated for 30 min exhibited loading increases of 68.5% at 0.15 bar and 8.7% at 1 bar relative to the prepared baseline, accompanied by an 8.6% decrease in descending-branch release over 1.0–0.1 bar. These descriptive observations emphasize the importance of specifying both pressure and the loading or release objective. Replication, pretreatment validation, extended desorption, and equilibration tests are required to establish reproducibility and the origin of retention.

The present evidence supports preliminary treatment comparisons under a defined pure-gas protocol. Validated textural measurements, repeated mixed-gas cycles, and carbon-balanced mineralization experiments would establish the broader material and process implications.

Author Contributions: Conceptualization, Y.L. and J.L.; methodology, Y.L.; software, D.J.; validation, J.L. and F.X.; formal analysis, Y.L.; investigation, D.J.; resources, Y.L. and J.L.; data curation, D.J.; writing—original draft preparation, Y.L.; writing—review and editing, Y.L. and Y.F.; visualization, Y.F. and P.X.; supervision, F.X.; project administration, F.X.; funding acquisition, Y.L. All authors have read and agreed to the published version of the manuscript.

Funding: This research was funded by the Deep Earth Probe and Mineral Resources Exploration—National Science and Technology Major Project of the Ministry of Natural Resources of the People's Republic of China, grant No. 2025ZD1010904, Open Foundation of State Key Laboratory of Mineral Processing, grant No. BGRIMM-KJSKL-2026-15, Fundamental Research Funds for the Central Universities, grant No. FRF-TP-26-039, and Foreign Expert Projects of the Ministry of Human Resources and Social Security, grant No. H20260488.

Data Availability Statement: The data used in this study is available from the corresponding author upon reasonable request.

Conflicts of Interest: The authors declare no conflicts of interest.

References

1. Li, J.; Hitch, M. Carbon Dioxide Sorption Isotherm Study on Pristine and Acid-Treated Olivine and Its Application in the Vacuum Swing Adsorption Process. *Minerals* **2015**, *5*, 259–275. [CrossRef]
2. Li, J.; Hitch, M. Carbon dioxide adsorption isotherm study on mine waste for integrated CO_2 capture and sequestration processes. *Powder Technol.* **2016**, *291*, 408–413. [CrossRef]
3. Li, J.; Hitch, M. Mechanical activation of ultramafic mine waste rock in dry condition for enhanced mineral carbonation. *Miner. Eng.* **2016**, *95*, 1–4. [CrossRef]
4. Kerisit, S.; Bylaska, E.J.; Felmy, A.R. Water and carbon dioxide adsorption at olivine surfaces. *Chem. Geol.* **2013**, *359*, 81–89. [CrossRef]

5. Ermolov, Y.; Vasilchenko, A.; Lazorenko, G. Anisotropy in Carbon Dioxide Adsorption on Forsterite. *Int. J. Mol. Sci.* **2024**, *25*, 12639. [CrossRef] [PubMed]
6. Thommes, M.; Kaneko, K.; Neimark, A.V.; Olivier, J.P.; Rodriguez-Reinoso, F.; Rouquerol, J.; Sing, K.S.W. Physisorption of gases, with special reference to the evaluation of surface area and pore size distribution (IUPAC Technical Report). *Pure Appl. Chem.* **2015**, *87*, 1051–1069. [CrossRef]
7. Sandvik, K.L.; Kleiv, R.A.; Haug, T.A. Mechanically activated minerals as a sink for CO_2. *Adv. Powder Technol.* **2011**, *22*, 416–421. [CrossRef]
8. Li, J.; Hitch, M. Characterization of the microstructure of mechanically-activated olivine using X-ray diffraction pattern analysis. *Miner. Eng.* **2016**, *86*, 24–33. [CrossRef]
9. Kleiv, R.A.; Thornhill, M. Mechanical activation of olivine. *Miner. Eng.* **2006**, *19*, 340–347. [CrossRef]
10. Kalinkina, E.V.; Kalinkin, A.M.; Forsling, W.; Makarov, V.N. Sorption of atmospheric carbon dioxide and structural changes of Ca and Mg silicate minerals during grinding: I. Diopside. *Int. J. Miner. Process.* **2001**, *61*, 273–288. [CrossRef]
11. Gamba, N.; Farina, V.; Garroni, S.; Mulas, G.; Gennari, F. CO_2 storage and conversion to CH_4; by wet mechanochemical activation of olivine at room temperature. *Powder Technol.* **2021**, *377*, 857–867. [CrossRef]
12. Julcour, C.; Bourgeois, F.; Bonfils, B.; Benhamed, I.; Guyot, F.; Bodénan, F.; Petiot, C.; Gaucher, É.C. Development of an attrition-leaching hybrid process for direct aqueous mineral carbonation. *Chem. Eng. J.* **2015**, *262*, 716–726. [CrossRef]
13. Cau, C.; Taras, A.; Masia, G.; Caggiu, L.; Enzo, S.; Garroni, S.; Murgia, F.; Mulas, G. Structural Evolution of Olivine during Mechanochemically Assisted Mineral Carbonation under CO_2 Flow. *Inorganics* **2024**, *12*, 269. [CrossRef]
14. Stillings, M.; Shipton, Z.K.; Lunn, R.J. Mechanochemical processing of silicate rocks to trap CO_2. *Nat. Sustain.* **2023**, *6*, 780–788. [CrossRef]
15. Haug, T.A.; Kleiv, R.A.; Munz, I.A. Investigating dissolution of mechanically activated olivine for carbonation purposes. *Appl. Geochem.* **2010**, *25*, 1547–1563. [CrossRef]
16. Sanna, A.L.; Carta, M.; Pia, G.; Garroni, S.; Porcheddu, A.; Delogu, F. Chemical effects induced by the mechanical processing of granite powder. *Sci. Rep.* **2022**, *12*, 9445. [CrossRef] [PubMed]
17. Gerdemann, S.J.; O'Connor, W.K.; Dahlin, D.C.; Penner, L.R.; Rush, H. Ex situ aqueous mineral carbonation. *Environ. Sci. Technol.* **2007**, *41*, 2587–2593. [CrossRef] [PubMed]

Disclaimer/Publisher's Note: The statements, opinions and data contained in all publications are solely those of the individual author(s) and contributor(s) and not of MDPI and/or the editor(s). MDPI and/or the editor(s) disclaim responsibility for any injury to people or property resulting from any ideas, methods, instructions or products referred to in the content.